INSTITUTE OF PHYSICS PUBLISHING JOURNAL OF PHYSICS D: APPLIED PHYSICS
J. Phys. D: Appl. Phys. **38** (2005) R253–R267 doi:10.1088/0022-3727/38/16/R01

TOPICAL REVIEW

Femtosecond ultraviolet photoelectron spectroscopy of ultra-fast surface processes

Michael Bauer

Fachbereich Physik, TU Kaiserslautern, 67663 Kaiserlautern, Germany

E-mail: mkbauer@physik.uni-kl.de

Received 18 July 2004, in final form 28 April 2005
Published 5 August 2005
Online at stacks.iop.org/JPhysD/38/R253

Abstract

Conventional ultraviolet photoelectron spectroscopy (UPS) has been successfully used for decades to study *static* electronic properties of surfaces and their interaction with adsorbates. The recent progress in the creation of femtosecond and attosecond VUV pulses by means of high-order harmonic generation (HHG) opens the potential to operate UPS in a time-resolved mode, which is capable of monitoring ultra-fast dynamical *changes* of surface properties. It is now possible to evaluate the temporal evolution of chemical surface reactions on their fundamental time scales.

This paper reviews technical aspects of time-resolved UPS and its application to the study of ultra-fast surface processes. Special emphasis is placed on the creation of ultra-short VUV pulses by means of HHG and also on the description of the stroboscopic experimental approach that enables temporal resolutions of the order of femtoseconds. This review will show that time-resolved UPS is indeed capable of probing with femtosecond resolution dynamic surface processes related, for example, to electronic excitations at surfaces or to the chemical state of adsorbates on a femtosecond time scale.

1. Introduction

Femtosecond Ti : Sapphire laser systems are proven tools for the study of real-time dynamic surface processes on ultra-short time scales. With these systems, the achievable time resolution is controlled by the ability of the laser to deliver short optical femtosecond pulses in a stable, reproducible manner. The wavelength regime accessible by a conventional short-pulse Ti : Sapphire oscillator lies typically between the near infrared and optical regions, down to wavelengths of 200 nm. In a photoemission (PE) experiment, this wavelength regime only probes a relatively restricted bandwidth of the surface electronic states, specifically those states located a few electronvolts around and above the Fermi edge. Therefore, most of the surface related PE studies using this kind of laser source are based on a two photon PE process and focus mainly on electronic excitations, excited (pumped) and probed by the fundamental, second and third harmonic of the 800 nm laser output (for an overview see, e.g. [1]). However, an extension of the excitation wavelengths into the VUV, EUV and x-ray regions for these experiments allows for direct access to much deeper electron levels. These deeper electron levels are important because they also contain information on the chemical or the magnetic state or the structure of the surface. Therefore, real-time observation of ultra-fast surface property changes, such as the surface chemical state, with femtosecond resolution is possible and these changes can, in principle, be monitored over their entire temporal evolution.

To achieve this, an amplifier system is needed to boost the peak power of a Ti : Sapphire oscillator several orders of magnitude, which then induces nonlinear optical effects, resulting in frequency conversion beyond the region accessible

by the non-amplified laser output. In the late eighties, Rhodes co-workers [2] and Manus co-workers [3] described for the first time the generation of high-order harmonics and reported the conversion of the amplifier output to ultra-short coherent light pulses in the VUV, EUV and the x-ray regions. Later, photon energies up to 700 eV were observed by this technique [4–6] and pulse widths as short as 200 as have been reported for these light bunches [7, 8]. It is this latter property, in particular, which makes high-order harmonic generation (HHG) a unique source for the study of dynamical processes when ultra-high temporal resolution is required. Therefore, using a high-order harmonic source in a surface science PE experiment within a pump–probe scheme provides exciting insights into dynamical surface processes on extremely short time scales, something which was not possible until recently.

Haight pioneered the use of HHG for surface related experiments by demonstrating that HHG can be used as a light source for valence- and core-level photoelectron spectroscopy (see figure 1 and [15]). At this point, he had already recognized the two main advantages of the high-order harmonic source compared with those of the conventional short wavelength light sources, namely, that the harmonic source is both a small-scale (table-top) and a *tunable* VUV source and that the short pulse structure of the photon pulse from the harmonic source is, in principle, capable of real-time experiments on a femtosecond time scale to study ultra-fast dynamic processes at surfaces.

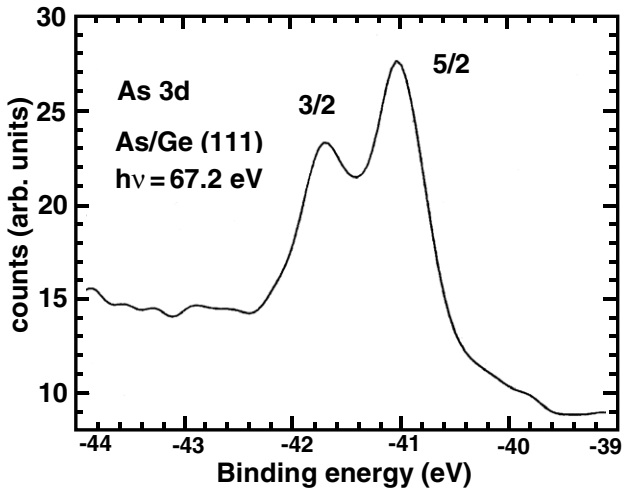

Figure 1. PE spectrum of the As 3d 3/2 and 5/2 spin-orbit split core states from a single monolayer of As deposited on Ge(111) recorded using an HHG source at a photon energy of 67.2 eV (from [51]).

In the first part of this review, a brief introduction to the principles of HHG will be given. This is followed by a description of the important aspects of the experimental set-up for time-resolved ultraviolet photoelectron spectroscopy (UPS), focusing on details such as wavelength selective UV optics and electron detection. In the third part of this review, static UPS results obtained with high-order harmonic sources will be discussed with an emphasis on the advantages of HHG in comparison with other UV sources. In the final section, time-resolved UPS measurements will be presented where electronic excitations as well as changes in the chemical state of a surface were successfully monitored.

2. High-order harmonic generation

HHG has been investigated both experimentally and theoretically in detail over the last two decades. The driving force for these studies was to investigate the fundamental nature of this highly nonlinear process and to evaluate the potential of HHG as an experimental tool in different research fields. Therefore, one of the goals of several of these studies is the improvement of the source specifications with respect to photon flux, photon energy, pulse width and the handling of the source to facilitate experimental use by 'non-experts'.

Next, the principle mechanism of HHG is qualitatively described. First, the illumination of an atom with a high intensity laser induces either multiphoton ionization at moderate intensities or tunnel ionization at high intensities ($>10^{14}\,\mathrm{W\,cm^{-2}}$ in the infrared regime) (see figure 2). Once free, the electron moves in the laser field $\vec{E}(t)$ and, when the laser field reverses, the electron can return to the ion core. One possible consequence of an electron–ion interaction at this point is the emission of high energy light, where the maximum achievable photon energy is limited only by the kinetic energy that the electron can accumulate during this optical half-cycle [9, 10]. For long laser pulses (>100 fs) and moderate intensities, this cut-off energy is given by $3.17U_p + E_0$, where $U_p = I/4\omega^2$ (atomic units) is the so-called ponderomotive energy, I and ω are the intensity and frequency of the electromagnetic field, respectively, and E_0 is the ionization potential

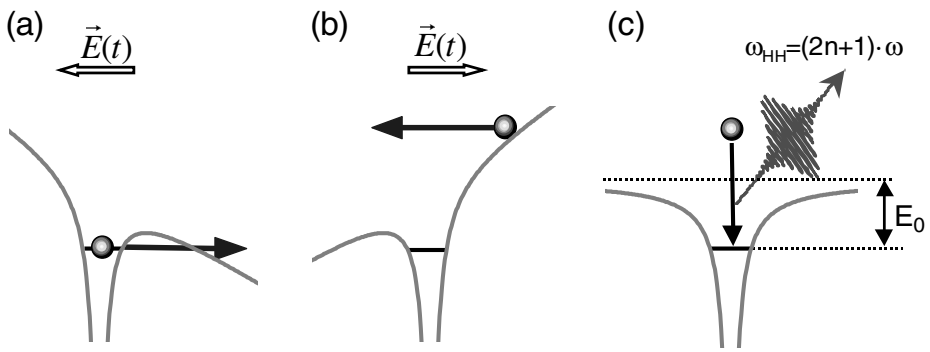

Figure 2. Series of events for HHG in the tunneling ionization regime: (*a*) owing to distortion of the atomic potential by an intense laser field, the electron can tunnel through the Coulomb barrier and is consequently accelerated away from the atomic core; (*b*) after reversal of the laser field, the electron returns to the ion and can (*c*) recombine with the atom, resulting in the generation of a photon at an odd harmonic frequency of the driving laser field.

of the atom. This relation is derived in a rather straightforward manner using a semi-classical approach, which considers the electrons released from the atomic potential due to ionization (see figure 2(*a*)) with no initial energy and at various times during the optical cycle of the laser field [11]. Solving the equation of motion for the electrons interacting with the oscillating electric field of the laser (see figures 2(*b*) and (*c*)) shows that the maximum kinetic energy of an electron when it returns to the nucleus is equal to $3.17U_P$. The spectral distribution of the emitted light consists of odd harmonics of the fundamental frequency ω, which reflects the periodicity of the creation process owing to the oscillating laser field. The restriction to odd multiples of ω results from the inversion symmetry of the isotropic gaseous medium [12]. A factor limiting the energy is the depletion of the ground state of the atom due to ionization before the laser pulse intensity reaches its maximum. The use of sub-100 fs lasers overcomes this intensity limit and enables the extension of the harmonic regime to even higher photon energies as a result of the nonadiabatic response of the atom to the fast rise time of the laser pulse [13]. In this way, the generation of harmonics in the water-window (280 eV $< h\nu <$ 540 eV) could be realized [4, 5] with energies approaching 800 eV [6].

Probably, the most surprising property of the harmonic spectrum is that the intensity of the harmonics does not generally decrease with increasing harmonic order [14]. Although the harmonic intensity decreases with harmonic order from the third to the eleventh order harmonic, higher harmonics, in contrast, do not follow this perturbative pattern. Instead, these high harmonics show a constant intensity regime known as the 'plateau', which extends to the cut-off region where the intensity decreases rapidly again. It is this special feature resulting from the non-perturbative character of the interaction that makes this type of UV source powerful enough to be used for photoelectron-spectroscopy over a wide photon energy range within the EUV region.

However, the efficiency and the cut-off energy of HHG depend on several factors including the gas species, focusing conditions [14] and the pulse width and chirp of the fundamental pulse [5]. With respect to the gas species, the atomic polarizability increases with atomic number; therefore, the highest conversion efficiencies are observed for the heavy noble gas species (Kr and Xe). On the other hand, the high ionization potential of the light noble metals allows for higher cut-off energies [15]. Typical harmonic spectra for different noble gases are shown in figure 3. Overall, conversion efficiencies per harmonic of 10^{-7}–10^{-8} have been achieved [16] and, for optimized conditions, efficiencies up to 10^{-5} have been reported [17, 18]. These conditions correspond to an effective photon flux of $>10^{10}$ photons/second using an input laser pulse energy of 150 μJ at a 1 kHz repetition rate.

The temporal characteristic of the emitted high-order harmonic pulses is a topic of recent interest wherein the harmonic pulse durations are calculated to be significantly shorter than the ultra-fast laser pulse and these calculations even predict the creation of attosecond pulses [19]. Earlier experiments confirm that the pulse duration is indeed shortened [20, 21].

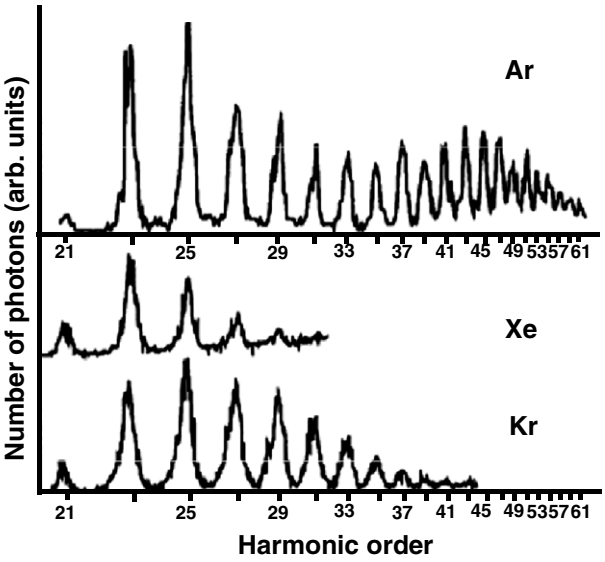

Figure 3. Harmonic spectra generated in different noble gases where the peak intensity of the fundamental laser is 5×10^{14} W cm^{-2}. Note that the relative intensities should not be directly compared (from [5]).

2.1. Attosecond EUV pulses

Very recently, several groups succeeded in the preparation and measurement of trains of attosecond harmonic pulses and single attosecond harmonic pulses [7, 8, 22]. These experiments paved the way for a new time regime. Attosecond pulses are generated by superimposing a comb of equidistant frequencies with an appropriate phase relationship, such as the spectral distribution obtained in the high-order harmonic plateau [7, 23–25]. The Fourier synthesis leads to the generation of a train of attosecond pulses separated by $2\pi/\omega_0$, where ω_0 corresponds to the spectral separation of the harmonics and is, therefore, twice the oscillation frequency of the fundamental laser pulse. Even a single attosecond EUV burst can be generated if an intense, low-cycle pump pulse is used. The single attosecond EUV burst results from the highly nonlinear dependence of HHG on the pump intensities in combination with the depletion of the neutral atomic ground state [26, 27]. Finally, the capability of these sources to perform time-resolved experiments on these extremely short time scales was demonstrated in quite a spectacular gas phase experiment [8, 28]. Two review papers on the topic of EUV attosecond pulses generated by means of HHG have been published recently [29, 30]. In the future, the use of these attosecond pulses in a PE experiment may provide exciting temporal probes for extremely short events, such as attosecond charge transfer processes or charge screening dynamics at surfaces.

3. Experimental and technical aspects for realizing time-resolved PE using high-order harmonics

An all-optical pump–probe scheme in the experimental design is necessary to make use of the extreme time resolution offered by the femtosecond temporal structure of the high-order harmonics in a time-resolved experiment. Figure 4

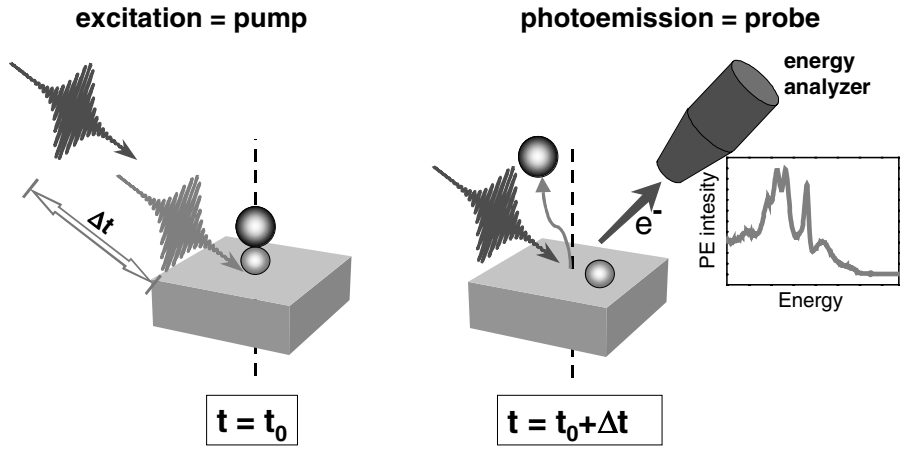

Figure 4. Principle scheme of a time-resolved PE experiment for monitoring ultra-fast surface processes. First, an ultra-short optical pump pulse initiates the dynamical process to be probed and defines the time-zero, t_0, of the measurement. Then a second ultra-short photon pulse arriving at the surface with a defined temporal delay, Δt, after excitation is used for the PE spectroscopy. The corresponding PE spectrum is characteristic for the state of the surface at $t_0 + \Delta t$. Repetition of the experiment at varying delay times Δt results in a series of photoelectron spectra reflecting the temporal evolution of the process originally initiated by the pump pulse.

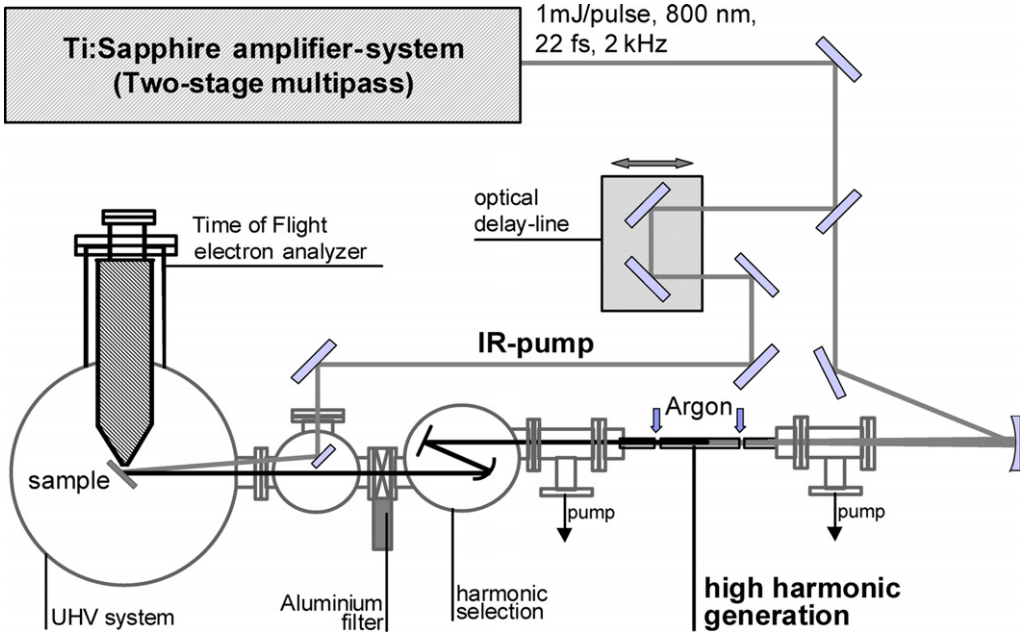

Figure 5. Scheme of an experimental set-up for time-resolved photoelectron spectroscopy using HHG.

demonstrates how such a scheme can be applied to a PE experiment to probe, for example, the dynamics of a chemical surface reaction. An intense, ultra-short laser pulse (typically the output of the amplifier system or its second harmonic) is used to excite the surface into a non-equilibrium state. The arrival time t_0 of the exciting (pump) pulse at the surface also defines the time-zero, t_0, of the experiment. At a certain time after excitation, $t_0 + \Delta t$, the HHG pulse arrives at the surface and a photoelectron spectrum is recorded where the recorded spectral distribution is characteristic for the chemical state of the surface at $t_0 + \Delta t$. Repetition of this experiment at subsequent time intervals allows for characterization of the sample state as it relaxes back into an equilibrium ground state. In principle, it is possible to monitor the entire temporal evolution of this process using this approach. It is important to note that the temporal resolution that can be achieved with this experiment is essentially determined by the temporal width of both the pump and the probe pulse. A schematic view of an experimental set-up for time-resolved photoelectron spectroscopy using HHG is shown in figure 5. Details of some of the key parts of the set-up, including the harmonic source, wavelength selection and electron spectrometer, are described in the following subsections.

3.1. High-order harmonic source

Experimentally, the generation of high-order harmonics requires both an intense short-pulse laser source and an interaction region/environment between the laser and the (noble)gas. Today, the most convenient way of generating

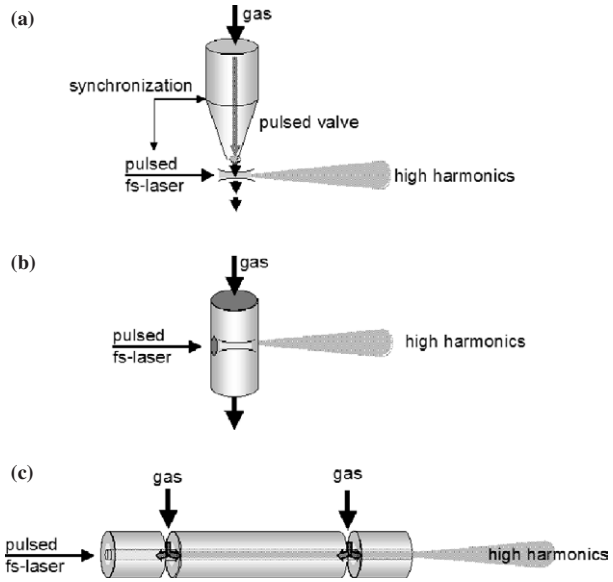

Figure 6. Different experimental schemes used for the generation of high-order harmonics with low gas loads on the rest of the vacuum system. (*a*) pulsed nozzle set-up; (*b*) thin tube perpendicular to IR and EUV propagation and (*c*) three-section hollow fibre set-up.

sufficient intense laser pulses for HHG are Ti : Sapphire laser systems based on chirped pulse amplification (for an overview see [31]). Commercial systems are nowadays available with pulse energies in the range of millijoules, output pulse width in the range of ten to some tens of femtoseconds and repetition rates up to several kilohertz.

A suitable interaction region between the laser and the atom, which delivers a sufficiently high gas pressure, can be created in different ways. In its simplest form, a constant gas flow is introduced into a gas cell. However, an important issue in the construction of such a cell is that the gas load for the rest of the system must be kept as low as possible, since VUV light is strongly absorbed in most materials and even the absorption owing to the propagation of the harmonic through the source gas can significantly reduce its intensity. For example, for an argon pressure of 5 mbar, only 10% of the light at a wavelength of 35 nm (∼35 eV) is transmitted over a distance of 1 cm [32]. A small gas load is even more important if the harmonic source is coupled to the ultra-high vacuum system used for surface science experiments as there is no conventional window available which transmits light in the EUV regime, but blocks the harmonic generation gas load from the UHV system.

By introducing a piezoelectric valve with a typical repetition rate of several hundred hertz, the average gas flow can be reduced significantly in comparison with a cell with a permanent gas flow ([33], see figure 6(*a*)). However, the closing cycles of the nozzle must be electronically synchronized with the clock speed of the pulsed laser to ensure that the maximum gas pressure occurs when the pulse arrives in the interaction region. This complication can be avoided if the set-up is designed such that the gas flows through a cell in the form of a thin tube where the thin tube is orthogonal to the plane generating the harmonics (figure 6(*b*)). In this design, the fundamental laser beam enters through a small hole on one side of the tube, and the harmonics leave the tube via a hole on the other side [34]. If the diameter of the entrance and exit holes for the laser and high-order harmonics are kept as small as possible (about 200 μm), then the gas load to the surrounding vacuum chamber is significantly reduced, while still allowing continuous gas flow through the tube. Alternatively, keeping the inner diameter of a three-section hollow fibre experimental set-up between 100 and 200 μm (figure 6(*c*)) produces a similar effect. In the hollow fibre configuration, the gas enters at the fibre intersections, which results in a constant gas pressure in the centre part of the fibre. Then, a small inner diameter on the other guarantees a high pressure gradient to the vacuum system and acts as a differential pumping stage. An additional advantage of the latter configuration is the increase in the interaction length between the laser and the gas as the beam is guided at high intensities through the hollow core fibre over a length of several centimetres. Phase velocities of both the fundamental beam and its harmonic are a function of the waveguide diameter and gas pressure and the phase velocities can, therefore, be adjusted to minimize the phase mismatch. This leads to a very long coherence and interaction length with a corresponding increase in conversion efficiency [35]. For other set-ups, the process of HHG is spatially restricted to the length of the focus in use.

3.2. *Spectral selection of harmonics*

For photoelectron spectroscopy, a defined photon energy is required that ideally shows an energy spread much smaller than the signature of interest in the photoelectron spectrum. Therefore, a certain energy range of the HHG source spectrum has to be selected. However, the bandwidth of the UV pulses simultaneously fixes the achievable temporal pulse-width of the UV bunch and, therefore, the maximum time resolution of the PE experiment. Therefore, a compromise between these two constraints (energy resolution and temporal resolution) must be found.

Reflection gratings are the most common method of wavelength selection where the gratings are arranged in a toroidal configuration that focuses the harmonic ray onto the sample. This approach is convenient for situations where the harmonic radiation is used for static spectroscopy or when the dynamics of interest require a time resolution of the order of picoseconds. The use of a grating allows for an easy tunability of the VUV source over a wide photon energy range, which is of particular advantage when compared with other selection techniques.

However, the diffraction of the specific wavelength by the grating into a finite order other than the specular reflex results in a tilt of the wave front with respect to the propagation direction. The resulting maximum path length difference between extreme rays is translated into an effective temporal broadening of the pulse perpendicular to the propagation direction (see figure 7, for a detailed discussion of this aspect see [36]). This effect can be quite critical for sub-100 fs pulses which have a longitudinal spatial extension that is less than 30 μm. Depending on the grating parameters, the temporal spread, $\Delta\tau$, owing to the wave-front tilt can be significantly larger than this distance. For a flat grating, $\Delta\tau$

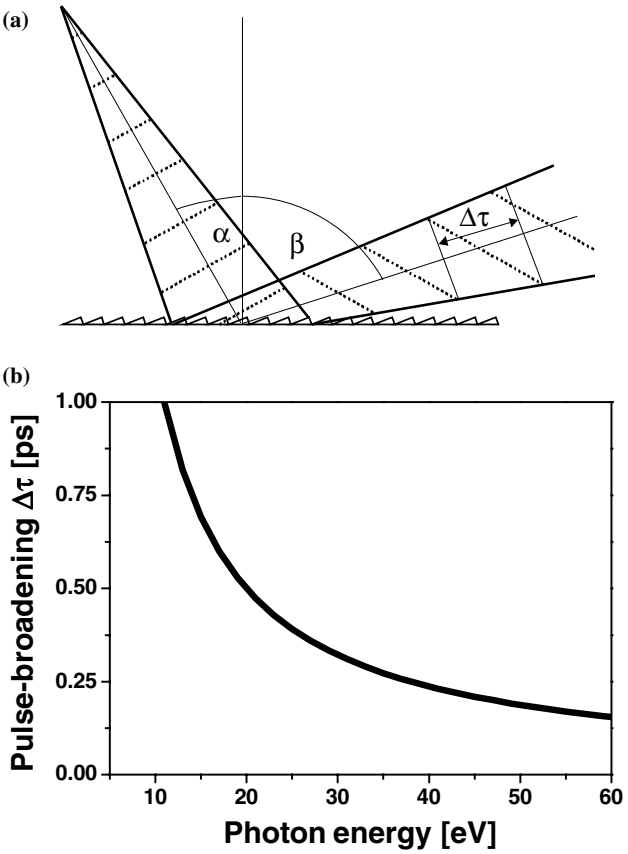

Figure 7. (*a*) Origin of the pulse width broadening, $\Delta\tau$, of a light pulse diffracted from a grating. The diffraction into a finite order m ($m \neq 0$) causes the wave-front to be tilted (- - - -) with respect to the propagation direction of the ray. (*b*) Pulse width broadening, $\Delta\tau$ induced by a flat grating as a function of the photon energy calculated using the following parameters: grating constant $d = 1.818\,\mu$m (550 goves/mm), angle of deviation $\theta = \alpha + \beta = 142^\circ$ and beam waist diameter at grating position $w = 2$ mm.

can be derived from the grating equation and is given by [37]:

$$\Delta\tau = \frac{N \cdot d}{c}[\sin(\alpha) - \sin(\beta)], \qquad (1)$$

where N is the number of illuminated grooves at the grating, d the grating constant, c the speed of light and α and β, the incidence angle and angle of diffraction, respectively, as defined in figure 7(*a*). Figure 7(*b*) displays the time-spread $\Delta\tau$ due to the wave-front tilt as a function of photon energy as calculated from equation (1) using the grating parameters and diffraction geometry described in the caption for figure 7. It is obvious that the effect of the wave-front tilt is most critical for the lower harmonics and that this effect significantly decreases as the harmonic order increases. However, the fact that an acceptable reflectivity of gratings in the sub-30 nm range requires additional grazing incidence conditions adds more restrictions and complexity to the design of the monochromator. Leone and co-workers [38] experimentally verified this grating dispersion effect for high-order harmonics and found a temporal spread of approximately 800 fs for the 17th harmonic using a toroidal grating (300 lines mm^{-1}, total diffraction angle of 172°). Reduction of the illuminated area, $N \cdot d$, by placing a 1 mm iris in front of the toroidal grating resulted in a decrease of the temporal spreading to 400 fs.

Compensation for the wave-front tilt can, in principle, be achieved by the use of two gratings in a compensated monochromator scheme as proposed by Villoresi [39]. In this scheme, two identical curved gratings are used to achieve the wavelength selection by diffraction from the first grating in combination with a slit located in its focal plan. The second grating is placed symmetrically with respect to the focal plane to compensate for the path length difference. Villoresi also calculated the effective group velocity dispersion (GVD) of this set-up, which is due to the pathlength difference of rays of different wavelengths. Even though it is not possible to completely compensate for both the GVD and the wave-front tilt in a two-grating set-up simultaneously, Villoresi found that the induced GVD is still quite low when the pathlength difference per nanometre is within 5 μm. For a typical spectral harmonic width of the order of 0.5 nm, this corresponds to a temporal spread of 15 fs.

Experimentally, a compensated (non-symmetrical) two-grating scheme for harmonic selection has been implemented in the experimental set-up used by the Leone group [38]. In this configuration, they were able to reduce the measured temporal width of the 17th harmonic from 400 fs using the single grating configuration to 180 fs using the compensated two-grating scheme.

Since the reflectivity of gratings in the VUV range is typically rather low and the compression performance of the two grating configuration quite sensitive to misalignments, a single grating set-up for harmonic selection may still be an interesting option. A scheme that should still be able to compensate for the wavefront tilt within such an approach has been proposed [40]. Instead of correcting the distortion of the harmonic (probe) beam, the propagation of the optical excitation (pump) pulse is adjusted. By correctly choosing the corresponding angle between the pump and probe beam, their wavefronts can be aligned parallely so that they hit the surface in parallel. This guarantees that the predefined temporal delay between the pulses is kept constant along the wavefront without affecting the (local) effective temporal width of the pulses. For other angles (e.g. in the case of a typically near-collinear arrangement) where this parallel alignment is not achieved, it is, in fact, this wavefront misfit that produces the main contribution to temporal broadening within a pump–probe experiment. More recently, a three-grating set-up has been proposed, which leaves the temporal structure of a selected harmonic pulse essentially undisturbed [41]. Ray tracing simulations indicate that the remaining stretching due to wave-front distortions is only about 1 fs.

Alternate optics that effectively select a restricted spectral regime of the harmonic spectrum are VUV or EUV multilayer mirrors. These UV and x-ray optics are equivalent to dielectric filters in the optical regime. They consist of a layered structure in which the optical constants vary periodically with depth, resulting in selective reflection of electromagnetic waves having particular wavelengths. In contrast to a diffraction grating design, wavelength selection results from interaction with the periodicity perpendicular to the surface plane reflection in the zeroth order (specular reflection). Therefore, the outgoing ray does not exhibit

the typical wave-front tilting seen with conventional gratings. These optics are particularly useful in extending the capability of time-resolved PE experiments to achieve time-resolved studies in the low femtosecond regime [42, 43] and even down to the attosecond regime [8]. Not only do the VUV and EUV multilayer mirrors leave the temporal characteristics of the UV pulses unchanged, they also have the advantage of quite high reflectivities having been achieved for specific spectral ranges. For example, silicon–molybdenum stacks, probably the most prominent type of multilayer mirror, can be produced to give reflectivities as high as 69% at a wavelength of 13.6 nm (91 eV) [44]. In addition, this value is not restricted to grazing incidence angles, but can also be specified for a wide range of angles including normal incidence, which makes this kind of optics quite convenient to align. A further benefit is that modifications in the stacking parameters can potentially be used to add a defined amount of positive or even negative dispersion to the reflected beam in a manner similar to dielectric mirrors in the optical regime. In this way, it may even be possible to compensate for the dispersion intrinsic to the harmonic spectrum itself [45].

There are, however, two main obstacles to the use of multilayer mirrors for wavelength selection. First, in the EUV/XUV regime, all materials absorb and this limits the number of layers that can contribute to the overall reflectance and also defines the selected spectral window. Second, roughness in combination with interdiffusion and alloying of the materials can potentially degrade the individual interfaces and their subsequent performance. Therefore, this restricts the number of materials that can be combined to manufacture a multilayer mirror with specific characteristics. A further drawback of multilayer optics, when compared with the selection gratings, is the limited tunability of the multilayer optics over a rather small wavelength regime, which makes these optics less flexible.

A different approach to harmonic selection described in the literature is the use of a laser pulse with a defined control of the temporal shape to drive the HHG process [46]. For example, femtosecond pulse-shaping, in combination with generic algorithms for optimization of a given process, has been applied to numerous applications in the past few years (see e.g. [47]) Specifically, Bartels *et al* [46] successfully demonstrated that harmonic selection is possible by means of this technique where they were able to increase the intensity of a selected harmonic by a factor of eight, whereas adjacent harmonic orders were only slightly enhanced.

3.3. Electron detection

Electron time-of-flight (ToF) techniques are typically required for efficient detection of the electrons photo-emitted from the sample because of the relatively low photon yield in combination with the pulsed nature of the high-order harmonic source at repetition rates of 1 kHz. In a conventional detection mode the read-out electronics enables detection of only a single electron per incident light-pulse, which limits the possible count rate to a maximum of approximately $\frac{1}{10}$ the repetition rate of the laser. Otherwise, detection of fast electrons (corresponding to the high energy side of the photoelectron spectrum) will be favoured in comparison with low energy electrons, resulting in significant distortions of the recorded photoelectron spectrum. This problem can be overcome by the use of a multi-hit per shot detection mode which increases the achievable count rate considerably. Multi-hit detection can either be achieved by the use of a multi-anode detector [48] or by the use of modern read-out and signal conversion electronics specified for a fast serial acquisition detection mode. Further improvement in detection efficiency can be achieved by the use of collimating electron optics. For example, parabolic electron mirrors and magnetic bottle ToF set-ups that allow for an efficient collection of emitted photoelectrons over a large solid angle have been successfully used for gas-phase PE experiments (see [38, 49]) and also in a restricted number of surface science experiments [50, 51]. If required, angular resolution can be conserved through the use of the multi-anode detection mode.

Using photon energies of the order of several tenths of an electronvolt, results in a maximum kinetic energy of electrons of the same magnitude. As the energy resolution, ΔE, of ToF detectors quadratically decreases with increasing kinetic energy of the electrons, care must be taken to ensure that ΔE is kept within an acceptable range. To ensure this, a sufficiently long electron drift tube, fast detection electronics (TDC) or retarding meshes in the drift tube may be used.

In the future, electrostatic electron analyzers equipped with two-dimensional detectors for *parallel* acquisition of a finite area in energy–momentum space may be used as an alternative scheme for high electron detection efficiency using low-repetitive light sources. The advantages of this type of a detector when compared with the conventional ToF spectrometers are a high energy resolution independent of the electron kinetic energy and the additional information depth with respect to momentum space. Figure 8 shows an example of a photoelectron spectrum from a Cu(111) surface that has been recorded with a two-dimensional hemispherical analyzer using the second harmonic of a low repetitive (1 kHz) laser-amplifier source.

4. PE using high-order harmonics

4.1. Static photoelectron spectroscopy using high-order harmonics

The easy tunability of high-order harmonic sources over a wide range of the EUV regime makes them an attractive alternative to conventional EUV sources in laboratory use. The broad spectral distribution of the high-order harmonic source within the accessible photon energy range (a range of several ten electronvolts) offers a flexibility close to that of a synchrotron source in this spectral regime. This feature is particularly important as cross-sections for PE depend critically on photon energy in the UV range and these cross-sections also contain valuable information on the surface properties under investigation. For example, resonance PE close to the absorption threshold of a core level can be used to enhance certain features in the valence band spectra or even to discriminate between possible excitation channels for the emission process [52]. From these so-called shape resonances in PE experiments, conclusions on the detailed orientation and bond length of a molecule can be drawn [53]. Wavelength

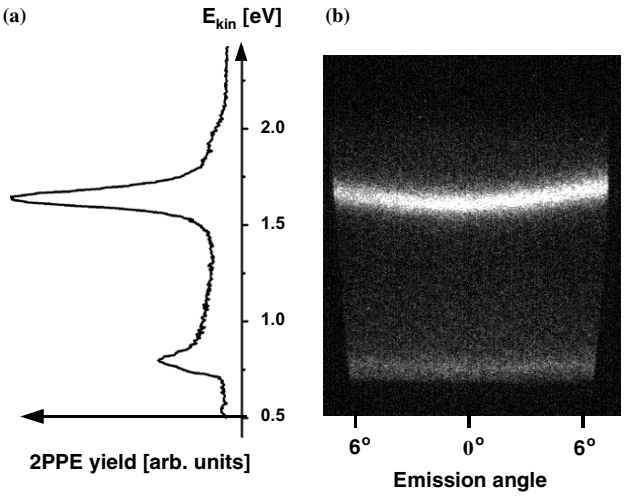

Figure 8. (2 Photon) Photoelectron spectrum from a Cu(111) single crystal surface recorded with a two-dimensional imaging hemispherical electron analyzer using the second harmonic from a low-repetitive (1 kHz) Ti : Sapphire laser system: (*b*) $E(k)$-map of the emitted electrons and (*a*) 2PPE spectrum taken from (*b*) corresponding to PE at normal emission. The pronounced (dispersing) feature at 1.6 eV corresponds to PE from the Shockley-type surface state of the Cu(111) surface. The photon pulse energy used in this *nonlinear* (2PPE) PE experiment was $<1\ \mu$J, which should be compared with the pulse energies in the range of nanojoules available from high-order harmonic sources for *linear* PE experiments.

tuning can also be used to enhance surface sensitivity as a result of the energy dependent escape depth of electrons [54]. Furthermore, dispersion effects as a function of the photon energy are useful for discriminating between bulk and surface states.

Figure 9(*a*) shows PE spectra of c(4 × 2)-2CO/Pt(111) for different photon energies that were obtained by Tsimilis *et al* [55] using a high-order harmonic source. For these measurements, excitation energy tuning was not only achieved by the selection of a single harmonic, but the harmonic spectral width of about 1 eV was also allowed for additional (continuous) tuning. Therefore, the spectra shown in figure 9(*a*) were recorded at photon energies that do not necessarily correspond to odd multiples of the fundamental wavelength of 800 nm ($h\nu = 1.55$ eV). In these spectra, a modulation in the relative peak intensities of the CO-induced 4σ, 5σ and 1π states is obvious. Figure 9(*b*) shows the corresponding PE cross-section for these peaks as a function of excitation energy. The 4σ and 5σ resonances located at photon energies of 37 eV and 28 eV, respectively, have been reported in an earlier publication [56] and can be assigned to shape resonances of the CO molecule [57]. In contrast, the 1π shape resonance has not been previously observed. Comparing this result with theoretical calculations [58] indicates that this feature is a result of an auto-ionization resonance of the CO molecule involving the 3σ and $2\pi^*$ states. In a separate report from the same group, low energy resonances arising from secondary electron emission in the HHG PE spectra for the clean Pt(111) were identified and attributed to the detailed band-structure above the vacuum level [59]. An important detail in the identification of these resonances was that the kinetic energy of the electrons emitted from this feature is independent of photon energy. Again, the key to a correct interpretation of these results was the tunability of the harmonic source used in these experiments.

Haight and Peale [60] used this flexibility to discriminate between the PE from the bulk and surface states of an As-terminated Ge(111) surface. Distinct features in the PE spectra are due to excitation from a bulk band dispersing in k, perpendicular to the surface plane and disperse, therefore, as a function of photon energy. Two other peaks at small binding energies do not disperse at all. Comparison of this observation with calculations of the surface band structure for this system allowed us to identify these features as As-derived electron states located at the surface. Haight and Seidler [61] also used a harmonic source for the spectroscopy of the localized and, therefore, narrow core-levels. For example, the 3/2–5/2 splitting of the Ga 3d core level of approximately 400 meV was clearly resolved. For spectroscopic experiments of the Pb 5d level, the tunability of the HHG source produced a significant cross-sectional enhancement of the PE signal from the core level by increasing the photon energy.

These examples illustrate how the harmonic source is roughly as flexible as the synchrotron sources for PE spectroscopy. Even though the HHG source flux is orders of magnitude smaller than what is possible for modern synchrotron sources, integration times for the PE results presented here are still convenient (a few minutes per spectrum). This means that a relatively inexpensive, table-top laboratory system can produce results for purely spectroscopic applications, comparable to those obtained using a synchrotron source with the added advantage of continuous access to the equipment.

4.2. Time-resolved PE experiments

The short pulse structure of the high-order harmonics enables the study of dynamic processes with a time resolution in the low femtosecond or, as recently demonstrated, even in the attosecond regime. In terms of the experimental design, a conventional set-up for photoelectron spectroscopy is used with an HHG source in combination with an all-optical pump–probe scheme. Only this configuration allows the high temporal resolution offered by the extremely short light pulses to be experimentally achieved.

Figure 5 shows an example of the experimental set-up for time-resolved UPS where this set-up uses a two-stage Ti : Sapphire multi-pass amplifier at 2 kHz repetition rate that can deliver 25 fs laser pulses with an energy of up to 1 mJ pulse^{-1} [43]. The short-pulse EUV source is a three-section capillary set-up for phase matched harmonic generation pumped by approximately 500 μJ from the amplifier. For argon, this produces a typical spectrum containing up to the 31st harmonic, which corresponds to a photon energy of 48 eV. A 200 nm thick aluminium filter placed between the harmonic source and the wavelength selection device blocks the transmission of the fundamental laser and also guarantees that the gas load from the harmonic cell is almost completely separated from the UHV chamber. Therefore, during operation, the pressure in the UHV chamber is maintained near 10^{-11} mbar. In this experimental set-up, harmonic selection is obtained by a pair of Mo/Si multilayer

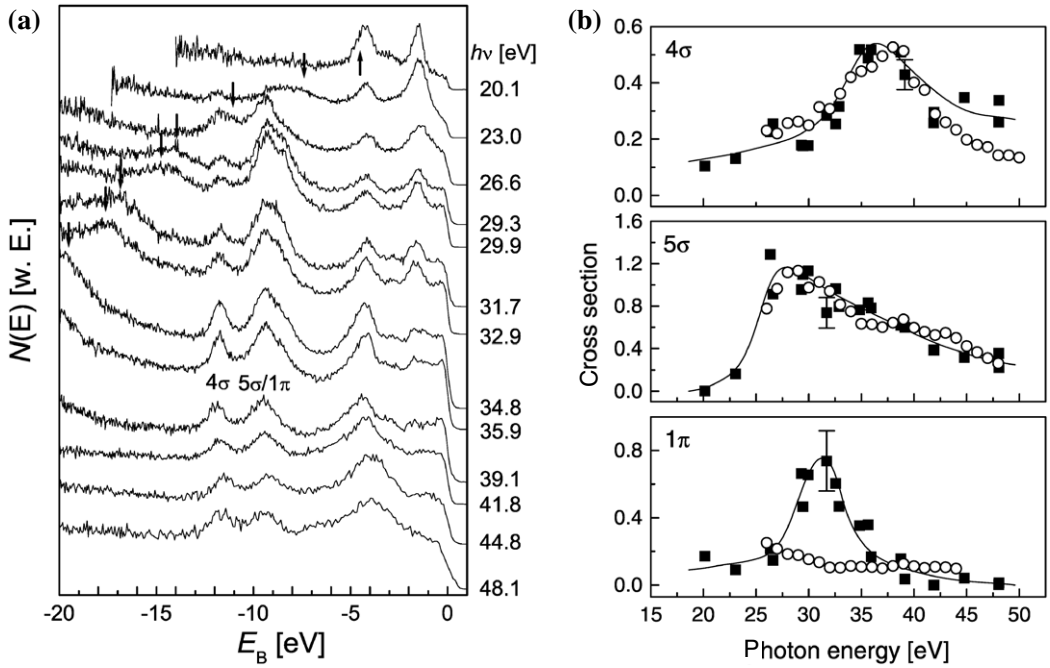

Figure 9. (*a*) UPS-spectra for c(4 × 2)–2CO Pt(111) in the $h\nu = 20$–50 eV range. The 4σ, 5σ and 1π valence resonances of the adsorbed CO exhibit a clear dependence on photon energy. (*b*) PE cross-section of the CO-induced 4σ, 5σ and 1π states for c(4 × 2)–2CO Pt(111) using p-polarized high-order harmonic radiation (■) The experimental results of [56] measured on Pt(110) have been added (○) (from [55]).

mirrors optimized for 42 eV, where the second mirror has a 1 m radius of curvature for focusing the EUV beam onto the surface. Photoemitted electrons are detected in a multi-hit ToF detection system with a 600 mm drift tube. PE spectra are recorded at a count rate of up to 8 kHz (4 counts/shot in average) without the significant spectral distortion that may result from the intrinsic dead time of the detection electronics. For time-resolved (pump–probe) experiments, part of the laser beam is picked up by a beam splitter and is then propagated over an optical delay stage to adjust the temporal delay Δt between the (fundamental) pump and (high-order harmonic) probe. Finally, the pump beam is focused slightly onto the sample to induce an excitation of the surface. The EUV pulse, following the pump beam at a defined temporal delay, Δt, is used to take a photoelectron spectrum that is characteristic of the surface state at $t_0 + \Delta t$. Successive changes in the temporal delay, Δt, between the pump and probe pulse allows us to sample, with femtosecond temporal resolution, the evolution of a given process from excitation to relaxation back to its ground state.

4.2.1. Probing electron excitations. The first time-resolved PE experiments using short-pulse VUV sources based on nonlinear processes, such as HHG, focused on the investigation of the decay dynamics of electronic excitations. In principle, photon energies in the optical and near UV regime are sufficient to probe excited electron distributions and their decay. For example, several studies using time-resolved 2PPE have been performed to study the relaxation dynamics of excited carriers in the low excitation density regime [1]. However, at increasing excitation densities, thermo- and multi-photon emission induced by the pump pulse becomes relevant and will, at some point, dominate the low energy spectrum of the electron distribution curve (EDC) (see figure 10 taken from [62]). Riffe *et al* [63] provides a quantitative discussion of the different effects involved in this type of process. In summary, the pump-pulse induced electron emission background can extend to quite high kinetic energies, up to several electronvolts, which means that the PE spectrum from a probe pulse with low photon energy can become completely blurred and any information on the excited state distribution and its decay will be lost. However, using the higher energy probe photons in the EUV regime removes the photoelectrons from this background to give a clear spectral distribution.

In earlier work, Haight and co-workers, in particular, focused on the investigation of carrier dynamics in a variety of semiconductor systems, such as InP(110), GaAs, Au/GaAs(110) and As-terminated Ge(111), which were close to the conduction minimum or inside the band gap. For semiconductors in this energy range the phase space for electron–electron scattering processes is quite limited and the decay of an excited electron distribution is determined by the electron lattice interaction (electron–phonon scattering). In these experiments, typical time scales for the energy relaxation were of the order of several picoseconds, so that the use of light pulses of several hundred femtoseconds and the use of reflective grating optics was not critical. A detailed overview and discussion of these works is given in [64]. Of particular interest are the results obtained regarding the excited carrier dynamics at a GaAs(110)-surface shown in figure 11 [65]. In this example, an *angular-resolution* mode of the electron spectrometer was efficiently used to probe the dynamics of population exchange between two separate points in momentum space as result of momentum transfer owing to the electron–phonon interaction. PE spectra recorded at different emission angles using 10.7 eV UV light showed

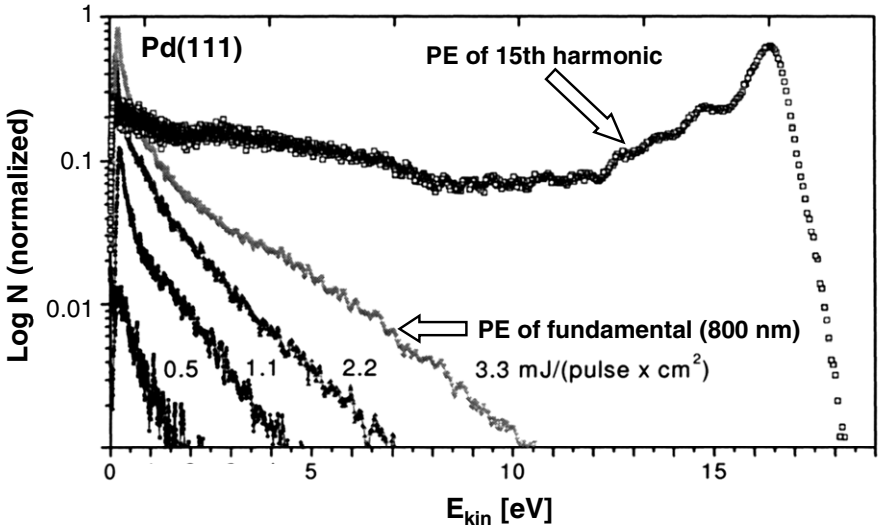

Figure 10. Example of high kinetic energy PE for a Pd(111) single crystal using different pump intensities of an 800 nm (1.55 eV) pump pulse. In comparison with the UPS spectrum (□) using the p-polarized 15th harmonic, PE up to several electronvolts is observed from the fundamental, which can exceed for low kinetic energy, in particular, the count rates achieved with the harmonic (from [62]).

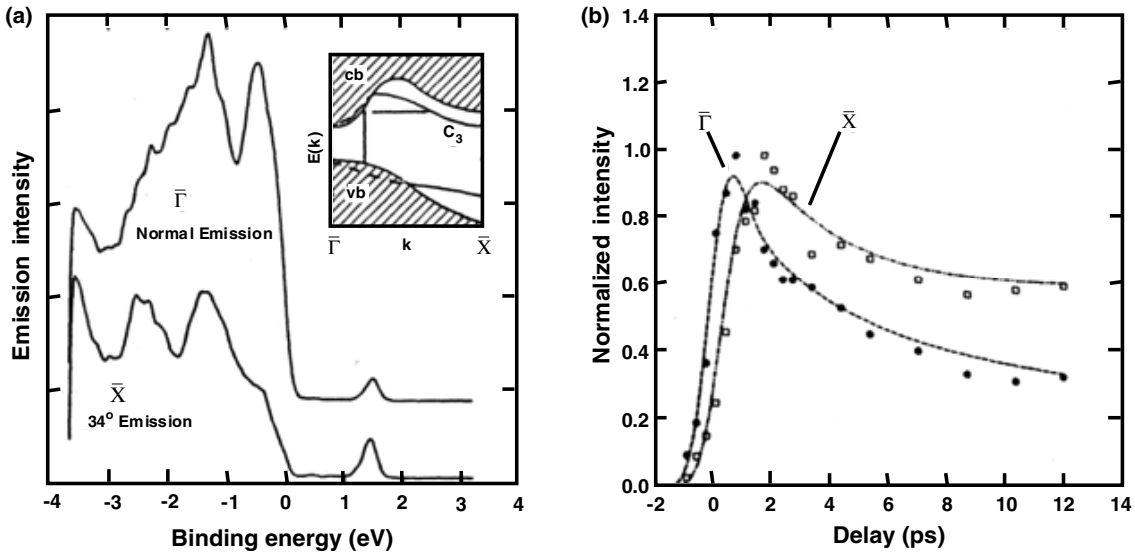

Figure 11. (*a*) Pump–probe PE spectra from cleaved GaAs(110). The bottom spectrum was collected at an emission angle of 34° relative to the surface normal in the $\bar{\Gamma}$–$\bar{X}$ direction. The top spectrum was collected along the surface normal corresponding to emission from $\bar{\Gamma}$. The peak appearing at a binding energy of about 1.5 eV is due to PE from electrons excited by the pump pulse. Inset: the relevant surface and bulk projected band structures (hatched regions); (*b*) Pump–probe delay curves for emission from $\bar{\Gamma}$ (●) and from $\bar{X}$ (○). Fits from the model calculations described in the text are shown as dashed ($\bar{\Gamma}$) and dot-dashed ($\bar{X}$) curves.

that the population of the GaAs $\bar{X}$-valley after absorption of the 700 nm pump beam is delayed by approximately 0.9 ps, with respect to the population of the $\bar{\Gamma}$-valley. This delay is related to inter-valley scattering from the $\bar{\Gamma}$- to the $\bar{X}$-point, which was induced by electron–phonon scattering. A rate equation model was fitted to the data which revealed that the characteristic scattering time, f, was approximately 0.4 ps. More recently, this set-up was used to investigate the decay of excited carriers in organic light emitting materials such as tris(8-hydoxy quinoline) aluminium (Alq) [66], where Alq is a material of interest for organic light emitting diodes (OLED). For these materials, the results show that the detailed decay processes are more complex and that other relaxation channels, such as Förster transfer, stimulated emission, concentration quenching and singlet–singlet excitation annihilation, have to be taken into account to explain the experimental findings.

In addition, the relaxation dynamics of highly excited electrons in an insulator (α-SiO_2) has been investigated in an 'inverted' UPS pump–probe scheme [67]. For this experiment, high-order harmonic radiation (25th harmonic) was used as the pump (exciting) pulse, where the fundamental and second harmonics of the amplifier output probed the population decay at 30 eV above the conduction band minimum. For harmonic selection, a boron–silicon multilayer mirror was used so that the temporal width of the pump–probe cross-correlation could be maintained at approximately 100 fs. The measured

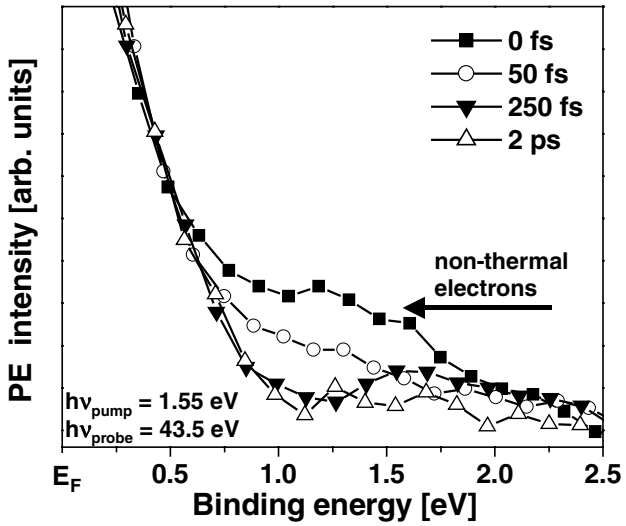

Figure 12. Ultra-fast decay of the non-thermal distribution of the electron gas, created by absorption of an intense pump laser pulse (800 nm, absorbed fluence 1 mJ cm^{-2} pulse^{-1}), probed with the 29th harmonic (43.5 eV). The non-thermal contribution (see arrow) has completely decayed 250 fs after the excitation (from [69]).

temporal decay in the population of these highly excited electrons lies within 10 ps and is due to both ejection of the electrons out of the solid and inelastic processes such as impact ionization. An important outcome from these data was that the upper limit for impact ionization rate was estimated to be about $\frac{1}{40}$ ps^{-1}, which is surprisingly small.

In contrast to semiconductors and insulators, the relaxation and thermal dynamics of excited electrons in metals after absorption of femtosecond pulses in the optical regime is much faster (from ten to a few hundred femtoseconds) [68]. Therefore, a study of these processes specifically requires the short-pulse characteristic of the high-order harmonics, which makes this source unique in comparison with alternative VUV sources. However, experiments focusing *in detail* on the relaxation of hot electron distributions at metal surfaces using high-order harmonics have not yet been carried out. Instead, the transient ultra-short signature at and above the Fermi edge related to the fast decaying hot electron distribution after absorption of the femtosecond pump pulse has been found to be quite useful in locating the temporal overlap in the fundamental pump and the EUV probe experiments. For transition metals, the lifetime of this distribution can be quenched down to the order of 10 fs, which makes it a good reference for estimating the upper time resolution limit for the optical pump/HHG probe experiment, particularly when non-dispersive harmonic selection is used. Siffalovic *et al* [42] found that after excitation of a Pt(110) surface with 800 nm light at an intensity of 2×10^{11} W cm^{-2} the induced non-equilibrium hot electron distribution probed by the high-order harmonic light had almost completely disappeared after 100 fs. Similar findings for Pt(111) have also been reported by Bauer and co-workers [69] using comparable pump intensities. As can be seen in figure 12, it was possible to observe significant changes in the hot (non-thermal) electron distributions for the first 50 fs after excitation, which gives an idea about the time resolution that can be achieved in these experiments. Note that for both studies, multilayer mirrors were used for harmonic selection. Even though this was not the focus of these studies, both results indicate that the decay of the non-thermal hot electron distribution in a transition metal such as Pt happens on a significantly shorter time scale than that for gold where thermalization times of the order of a few hundred femtoseconds were found [68]. In comparison with gold, the much higher density of d-electronic states around the Fermi edge of platinum increases the phase space for electron–electron scattering and accounts for these observations.

4.2.2. Time-resolved valence and core-level spectroscopy. Experiments using harmonic sources for both conventional photoelectron spectroscopy and for probing the decay dynamics of electronic excitations at surfaces complement experiments performed with alternate photon sources, such as synchrotron light (UPS) and femtosecond pulses in the optical regime (2PPE). However, in both cases, the full potential of high-order harmonic sources, i.e. the capability to deliver *(sub-)femtosecond pulses* at photon energies in the *EUV regime*, is not fully realized. Indeed, the combination of these two properties enables monitoring, with femtosecond resolution, of the time-dependent changes to the valence- and core-level electronic structure of a surface. In other words, the electronic levels that contain information on the chemical bond between a molecule and a surface can be examined. Therefore, a time-resolved PE experiment using high-order harmonics provides insight into the dynamics of surface chemical processes on their fundamental time scales. In the final part of this section, two recent experiments are reviewed that successfully show how high-order harmonics were applied to the study of dynamic surface processes by monitoring transient changes in the valence and core electronic structure, respectively, on a femtosecond time scale. In both cases, photon energies in the EUV regime were used, at $h\nu \approx 40$ eV and $h\nu \approx 70$ eV, respectively.

In the first experiment, the observed changes in the spectral distribution of a valence orbital for molecular oxygen adsorbed on Pt(111) are assigned to changes in the chemical state of the adsorbate on a time scale of only a few hundred femtoseconds (see figure 13) [69, 70]. In this case, the sample under investigation was prepared by adsorbing a saturation layer of molecular oxygen onto a Pt(111) substrate maintained at a surface temperature of 77 K. These conditions result in the superoxo sites on the platinum surface predominantly occupied by the oxygen. The characteristic feature of interest for the oxygen chemical state appears at a binding energy of about 6 eV, with respect to E_F in the UPS spectrum, which corresponds to PE from the 1π orbital of the oxygen. Next, a chemical transition of the oxygen is induced as it couples with the Pt substrate after absorbing an intense femtosecond laser pump-pulse (absorbed fluence: 1 mJ cm^{-2} pulse^{-1}) that efficiently excites/heats the electron gas. Specifically, the authors observe the instantaneous creation of a non-thermal electron distribution in the platinum substrate, which decays on a time scale of approximately 200 fs. Simultaneously, a change in the spectral characteristics of the oxygen 1π orbital appears in the spectral distribution, where this change is significantly delayed, with respect to the pump excitation and does not appear before, approximately 100 fs have passed. Using a Lorentzian to fit this feature for different time delays indicates

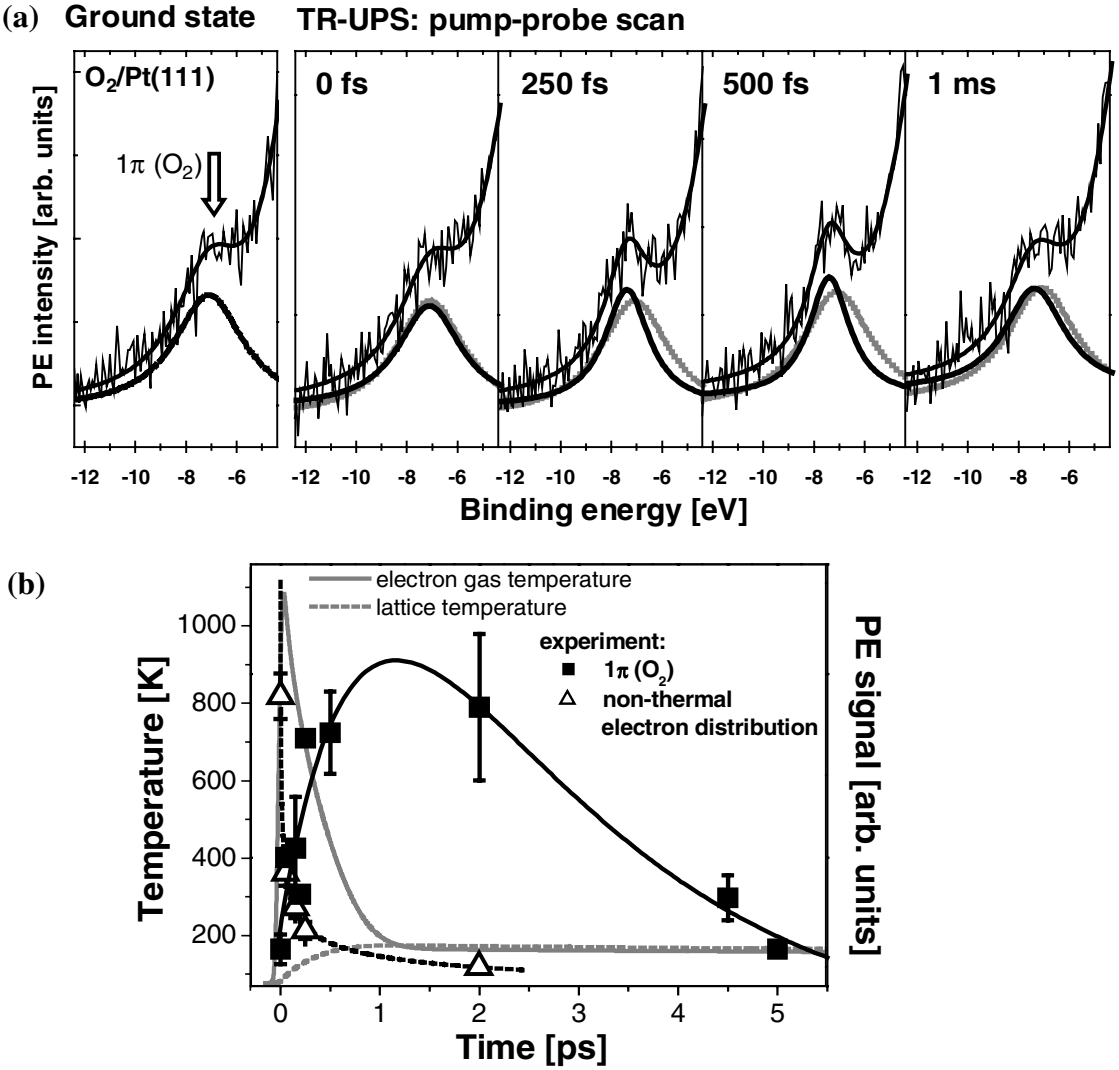

Figure 13. Time-resolved PE results from a saturation layer of molecular oxygen adsorbed on a Pt(111) surface. (*a*) PE spectra obtained for the ground state of the system and at four different temporal delays. The shoulder (or peak) appearing in the spectra in the energy region between 6 and 8 eV binding energy is due to PE from the 1π-orbital of the oxygen. Transient changes observed in this region can be assigned to an excitation from the superoxo ground state of the oxygen into a peroxo excited state. The full black lines are Lorentzian fits to the data in comparison with a Lorentzian fit of the ground state spectrum (grey line). (*b*) Signal intensity as a function of temporal delay for a binding energy of ∼7 eV (■) reflecting the transient dynamics associated with the oxygen molecule. In addition, the decay dynamics of the non-thermal distribution for the electron sub-system of the substrate is included in the graph (△). Grey lines show the calculated transient changes in the temperature of the electron gas (——) and the lattice temperature (- - - -).

a continuous shift of the oxygen 1π feature to higher binding energies and a narrowing of its line width as the time delay increases to 1 ps. For longer times (several picoseconds), an almost complete recovery of the original (time zero) signal is observed, indicating that the observed chemical modification is mainly of a transient nature. However, this recovery is not fully complete as a permanent (non-reversible) change of the spectral characteristics of the oxygen is observed for prolonged interaction times. This is an indication that, in addition to relaxation into the original ground state configuration (superoxo oxygen), an alternative decay channel into a different, stable oxygen configuration is possible for the transient chemical oxygen state. Comparing this result with the static UPS-spectra obtained for molecular oxygen adsorption at low coverages shows that this second relaxed state corresponds to the peroxo state of oxygen on Pt(111).

Next, comparison of the time evolution of the PE signal with model calculations of the transient electron gas temperature and lattice temperature using a two-temperature model shows that the transient excitation of the molecular oxygen is, in this case, induced by the coupling of the adsorbate and the hot electron distribution. However, these results also show that the transient molecular oxygen state is not influenced by interactions with the lattice, which heats and cools on a much longer time scale than that for the transient states of the adsorbate.

In another time-resolved PE experiment, Siffalovic *et al* [71] monitored surface photovoltage transients on p-GaAs after photoexcitation of electrons from the valence into the conduction band using an intense 400 nm femtosecond pump-pulse. For these experiments, they used <100 fs EUV pulses with a photon energy of about 70 eV. The carrier

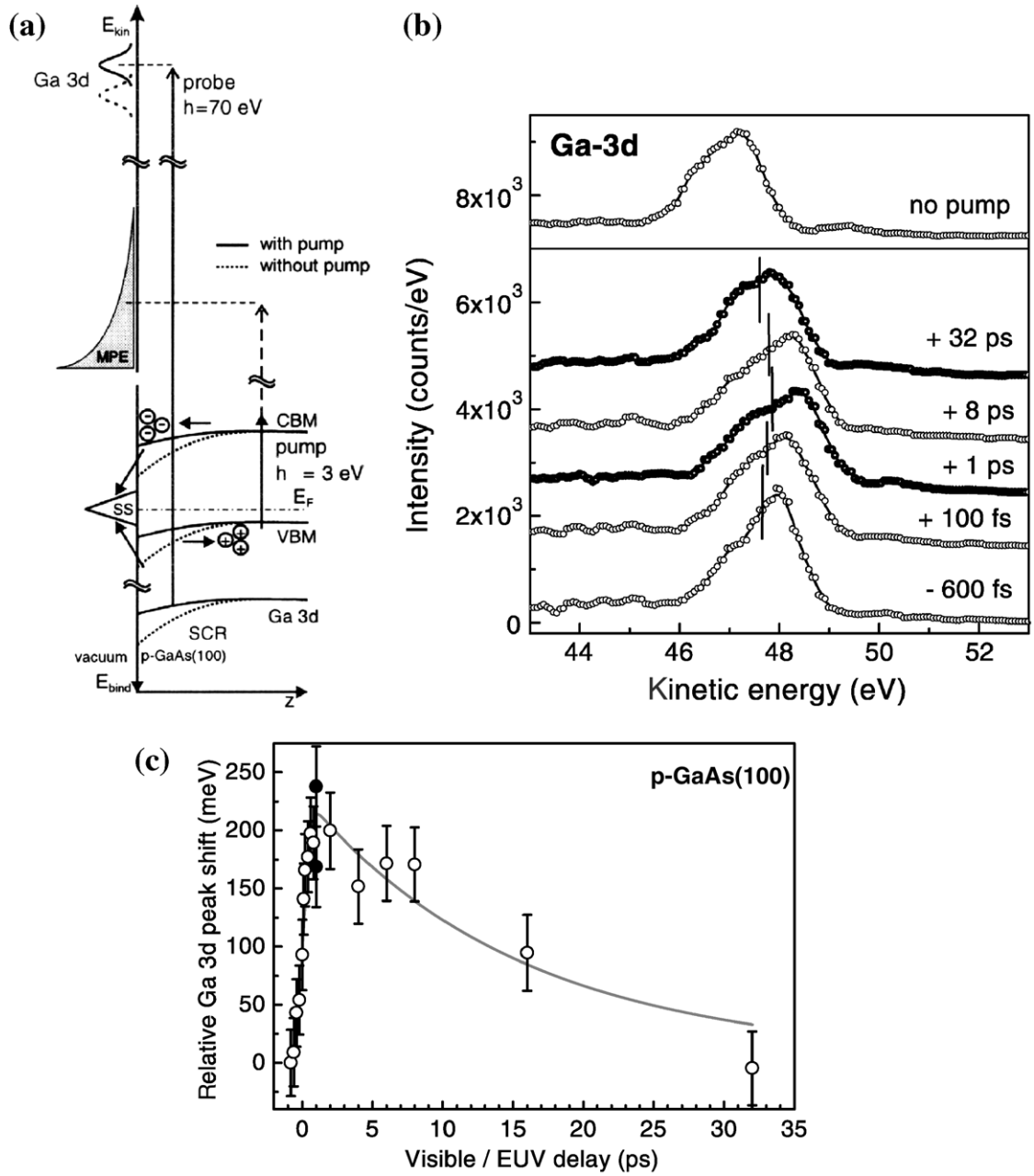

Figure 14. (*a*) Principle of the band bending variation after photoexcitation of p-GaAs detected by measuring the kinetic energy of the photoelectrons from the Ga-3d shell (for details see text). (*b*) Surface photovoltage transient in p-GaAs(100) revealed by a Ga-3d core-level shift as a function of the pump–probe delay within a TR-UPS experiment. The thin vertical lines show the peak's centre of gravity. (*c*) Temporal evolution of the centre of gravity of the Ga-3d line (○) after pulsed photoexcitation of the p-GaAs(100) crystal (from [71]). The two closed symbols correspond to experimental data taken at a delay of +1 ps at different times from the start of the experiment to check for the influence of systematic errors.

transport dynamics between the bulk and surface regions and the carrier recombination at the surface were probed by monitoring transient shifts of the Ga-3d core levels (binding energy ≈20 eV). The corresponding kinetic energy of the photoemitted electrons (≈50 eV) guarantees an exceptionally high surface sensitivity, as this energy is located right at the minimum of the mean-free path of electrons in solids [54] and has, therefore, an enhanced sensitivity to the surface photovoltaic effect. Furthermore, the relevant spectral probe feature is by this means sufficiently retracted from the PE background induced by the intense pump pulse (10 GW cm^{-2}) extending to kinetic energies of up to 10 eV, which would otherwise significantly blur the signal.

To understand the dynamic processes in the p-GaAs surface region induced by the absorption of the pump-pulse, the static electronic structure in the vicinity of the surface has to be considered (figure 14(*a*)). The excess charge associated with the existence of GaAs surface states located within the bandgap is compensated by a thin space charge region of a few nanometres, which leads to band bending in this area compared with the bulk band. Absorption of light results in the creation of free carriers (electrons in the conduction band and holes in

the valence band), which are then accelerated by the surface potential towards the surface (for the electrons) and into the bulk (for the holes), respectively. This charge redistribution in the surface layer results in a transient reduction in the band bending that can be monitored by tracking the corresponding energy shift in the binding energy of the 3d core levels of the Ga atoms located inside the space charge layer. In figure 14(*b*), the corresponding photoelectron spectra are displayed as function of temporal delay between pump and EUV probe pulse. The observed shifts in the centre of gravity of the Ga-3d peak reflect the dynamics related to the discharging and recharging of the surface layer owing to the transient charge redistribution. A fast carrier transport to the surface layer is indicated by a fast peak shift (within approximately 500 fs) to lower binding energies (figure 14(*c*)). However, the relaxation into the surface layer ground state occurs on much longer time scales (about 15 ps) and is driven by recombination processes and trapping of the electrons in surface states.

5. Concluding remarks

As an extension to conventional photoelectron spectroscopy, which is the present technique of choice for probing electronic band-structure and related bulk and surface properties, time-resolved photoelectron spectroscopy has the potential to become one of the leading ultra-fast dynamical probes for such diverse processes as surface femto-chemistry, ultra-fast magnetization or laser-induced structural phase transitions. Therefore, the experiments reviewed here, particularly those focusing on sub-picosecond dynamics, can be regarded as a starting point to this novel and evolving research field.

This review has focused on the most recent developments of time-resolved UPS at surfaces and has emphasized the importance of HHG for creating the ultra-short light pulses necessary for achieving the time-resolution required for the study of ultra-fast dynamical processes. By extending the photon energy range into the x-ray regime, it will, in the future, also be possible to address the deeper core levels by means of time-resolved XPS experiments. These core levels contain additional information on the surface electronic state and other related surface properties, which is complementary to information gained from the valence levels. A milestone in this direction has been realized recently with the creation of sub-femtosecond x-ray pulses at photon energies >1 keV using a laser-driven high-order harmonic process [72]. In addition, parallel to these table-top experiments, the next generation free electron lasers (FEL) can potentially deliver VUV and soft x-ray pulses in the sub-100 fs regime. It is the high brightness and capability for continuous tunability of these sources, in particular, that offers flexibility in their use for time-resolved PE not possible in laboratory experiments, even though experimental challenges such as the jitter-free temporal synchronization of the laser-pump and the FEL probe pulse with an accuracy of the order of femtoseconds and the temporal characterization of the FEL light bunch must first be solved. In addition to the current pump–probe experiments using conventional synchrotron sources [73], the experience gained over the last few years with laser-based table-top experiments will provide the foundation for the knowledge necessary to realize the first femtosecond FEL pump–probe experiments.

Acknowledgments

The author would like to thank T Lei, K Read, R Tobey, M M Murnane, H Kapteyn, J Beesley, P Zhou, M Aeschlimann, D v d Linde and S Mathias for their contribution to some of the experimental results reported here. In addition, the author is grateful to M Aeschlimann and J Dean for critical comments on various aspects of this manuscript.

References

[1] Petek H and Ogawa S 1997 *Prog. Surf. Sci.* **56** 239
[2] McPherson A, Gibson G, Jara H, Johann U, Luk T S, McIntyre I, Boyer K and Rhodes C K 1987 *J. Opt. Soc. Am.* B **4** 825
[3] Ferray M, L'Huillier A, Li X F, Lompré L A, Mainfray G and Manus C 1988 *J. Phys. B: At. Mol. Opt. Phys.* **21** L31
[4] Spielmann Ch, Burnett N H, Sartania S, Koppitsch R, Schnürer M, Kann C, Lenzner M, Wobrauschek P and Krausz F 1997 *Science* **278** 661
[5] Zhou J, Paetross J, Murnane M M, Kapteyn H C and Christov I P 1996 *Phys. Rev. Lett.* **76** 752
[6] Seres E, Seres J, Krausz F and Spielmann Ch 2004 *Phys. Rev. Lett.* **92** 163002
[7] Paul P-M, Toma E-S, Breger P, Mullot G, Auge F, Balcou P, Muller H-G and Agostini P 2001 *Science* **292** 1689
[8] Hentschel M, Kienberger R, Spielmann Ch, Reider G A, Milosevic N, Brabec T, Corkum P, Heinzmann U, Drescher M and Krausz F 2001 *Nature* **414** 509
[9] Krause J L, Schafer K J and Kulander K C 1992 *Phys. Rev. Lett.* **68** 3535
[10] Corkum P B 1993 *Phys. Rev. Lett.* **71** 1994
[11] Schafer K J, Krause J L and Kulander K C 1994 *Laser Interactions with Atoms, Solids and Plasmas* ed R M More (New York: Plenum) p 95
[12] Li X F, L'Huillier A, Ferray M, Lompré L A and Mainfray G 1997 *Phys. Rev.* A **39** 5751
[13] Christov I P, Zhou J, Paetross J, Rundquist A, Murnane M M and Kapteyn H C 1996 *Phys. Rev. Lett.* **77** 1743
[14] L'Huillier A and Balcou P 1993 *Phys. Rev. Lett.* **70** 774
[15] Haight R and Peale D R 1994 *Rev. Sci. Instrum.* **65** 1853
[16] Schnürer M, Cheng Z, Hentschel M, Tempea G, Kálmán P, Brabec T and Krausz F 1998 *Phys. Rev. Lett.* **83** 722
[17] Rundquist A, Durfee Ch G III, Chang Z, Herne C, Backus S, Murnane M M and Kapteyn H C 1998 *Science* **280** 1412
[18] Hergott J-F, Kovacev M, Merdji H, Hubert C, Mairesse Y, Jean E, Breger P, Agostini P, Carré B and Salières P 2002 *Phys. Rev.* A **66** 021801
[19] Schafer K J and Kulander K J 1997 *Phys. Rev. Lett.* **78** 638
[20] Glover T E, Schoenlein R W, Chin A H and Shank C V 1996 *Phys. Rev. Lett.* **76** 2468
[21] Bouhal A, Salières P, Breger P, Agostini P, Hamoniaux G, Mysyrowicz A, Antonetti A, Constantinescu R and Muller H G 1998 *Phys. Rev.* A **58** 389
[22] Papadogiannis N A, Witzel B, Kalpouzos C and Charalambidis D 1999 *Phys. Rev. Lett.* **83** 4289
[23] Hänsch T W 1990 *Opt. Commun.* **80** 71
[24] Farkas Gy and Tóth Cs 1992 *Phys. Lett.* A **168** 447
[25] Papadogiannis N A, Witzel B, Kalpouzos C and Charalambidis D 1999 *Phys. Rev. Lett.* **83** 4289
[26] Schafer K J and Kulander K C 1997 *Phys. Rev. Lett.* **78** 638
[27] Christov I P, Murnane M M and Kapteyn H C 1997 *Phys. Rev. Lett.* **78** 1251
[28] Drescher M, Hentschel M, Kienberger R, Uiberacker M, Yakovlek V, Sctinizi A, Westerwalbesloh T, Kleineberg U, Heinzmann U and Krausz F 2002 *Nature* **419** 803
[29] Reider G A 2004 *Phys. J. D: Appl. Phys.* **37** R37
[30] Agostini P and DiMauro L F 2004 *Rep. Prog. Phys.* **67** 813
[31] Backus S, Durfee C G III, Murnane M M and Kapteyn H C 1998 *Rev. Sci. Instrum.* **69** 1207

[32] Henke B L, Gullikson E M and Davis J C 2002 *X-Ray Interaction with Matter* Berkley Laboratories, http://www-cxro.lbl.gov/optical_constants/intro.html
[33] Cross J B and Valentini J J 1982 *Rev. Sci. Instrum.* **53** 38
[34] Macklin J J, Kmetec J D and Gordon C L III 1993 *Phys. Rev. Lett.* **70** 766
[35] Rundquist A, Durfee Ch G III, Chang Z, Herne C, Backus S, Murnane M M and Kapteyn H C 1998 *Science* **280** 1412
[36] Villoresi P 1999 *Appl. Opt.* **38** 6040
[37] Born M and Wolf E 1980 *Principles of Optics* (Oxford: Pergamon)
[38] Nugent-Glandorf L, Scheer M, Samuels D A, Bierbaum V and Leone S R 2002 *Rev. Sci. Instrum.* **73** 1875
[39] Villoresi P 2000 *Laser Part. Beams* **18** 529
[40] Zacharias H 2001 private communications
[41] Norin J, Osvay K, Albert F, Descamps D, Yang J, L'Huillier A and Wahlström C-G 2004 *Appl. Opt.* **43** 1072
[42] Siffalovic P, Drescher M, Spieweck M, Wiesenthal T, Lim Y C, Weidner R, Elizarov A and Heinzmann U 2001 *Rev. Sci. Instrum.* **72** 30
[43] Bauer M, Lei C, Tobey R, Murnane M M and Kapteyn H 2003 *Surf. Sci.* **532–535** 1159
[44] Braun S, Mai H, Moss M, Scholz R and Leson A 2002 *Japan. J. Appl. Phys.* **41** 4074
[45] Norin J *et al* 2002 *Phys. Rev. Lett.* **88** 193901
[46] Bartels R, Backus S, Zeek E, Misoguti L, Vdovin G, Christov I P, Murnane M M and Kapteyn H C 2000 *Nature* **406** 164
[47] Judson R S and Rabitz H 1992 *Phys. Rev. Lett.* **68** 1500
Yelin D, Meshulach D and Silberberg Y 1997 *Opt. Lett.* **22** 1793
Assion A, Baumert T, Bergt M, Brixner T, Kiefer B, Seyfried V, Strehle M and Gerber G 1998 *Science* **282** 919
[48] Haight R, Silberman J A and Lilie M I 1988 Rev. Sci. Instrum. **59** 1941
[49] Hansch P, Norby J R, Evans S H and Van Woerkom L D 1995 *Rev. Sci. Instrum.* **66** 5512
[50] Busolt U, Cottancin E, Röhr H, Socaciu L, Leisner T and Wöste L 1999 *Appl. Phys.* B **68** 453
[51] Haight R 1996 *Appl. Opt.* **35** 6445
[52] Hüfner S 1995 *Photoelectron Spectroscopy* (Berlin: Springer)
[53] Freund and Gustafsson T 1980 *Surf. Sci.* **94** 593
[54] Seah M P and Dench W H 1979 *Surf. Interface Anal.* **1** 2
[55] Tsimilis G, Kutzner J and Zacharias H 2003 *Appl. Phys.* A **76** 743
[56] Bare S R, Griffiths K, Hoffmann P, King D A, Nyberg G L and Richardson N V 1982 *Surf. Sci.* **120** 367
[57] Davenport J W 1976 *Phys. Rev. Lett.* **36** 945
[58] Stener M and Decleva P 2000 *J. Chem. Phys.* **112** 10871
[59] Tsilimis G, Fecher G H, Braun J, Kutzner J and Zacharias H 2004 *Appl. Phys.* A **78** 177
[60] Haight R and Peale D R 1993 *Phys. Rev. Lett.* **25** 3979
[61] Haight R and Seidler P F 1994 *Appl. Phys. Lett.* **65** 517
[62] Beesley J 2003 *PhD Thesis* University of Kaiserslautern
[63] Riffe D M *et al* 1993 *J. Opt. Soc. Am.* B **10** 1424
[64] Haight R 1995 *Surf. Sci. Rep.* **21** 275
[65] Haight R and Silbermann J A 1989 *Phys. Rev. Lett.* **62** 815
[66] Read K, Karlsson H S, Murnane M M, Kapteyn H C and Haight R 2001 *J. Appl. Phys.* **90** 294
[67] Quéré F, Guizard S, Martin Ph, Petite G, Merdji H, Carré B, Herfott J-F and Le Déroff L 2000 *Phys. Rev.* B **61** 9883
[68] Fann W S, Storz R, Tom H W K and Bokor J 1992 *Phys. Rev. Lett.* **68** 2834
[69] Lei C, Bauer M, Read K, Tobey R, Liu Y, Popmintchev T, Murnane M M and Kapteyn H C 2002 *Phys. Rev.* B **66** 245420
[70] Bauer M, Lei C, Read K, Tobey R, Gland J, Murnane M M and Kapteyn H C 2001 *Phys. Rev. Lett.* **87** 025501
[71] Siffalovic P, Drescher M and Heinzmann U 2002 *Europhys. Lett.* **60** 924
[72] Seres J, Seres E, Verhoef A J, Tempea G, Streli C, Wobrauschek P, Yakovlev V, Scrinzi A, Spielmann C and Krausz F 2005 *Nature* **433** 596
[73] Widdra W *et al* 2003 *Surf. Sci.* **543** 87